RESEARCH ARTICLE

Synoptic analysis and simulation of an unusual dust event over the Atacama Desert

Mark Reyers[1] 🄍 | **Mehdi Hamidi[2]** | **Yaping Shao[1]**

[1]Institute for Geophysics and Meteorology, University of Cologne, Cologne, Germany

[2]Faculty of Civil Engineering, Babol Noshirvani University of Technology, Babol, Iran

Correspondence
Mark Reyers, Institute for Geophysics and Meteorology, University of Cologne, Pohligstraße 3, 50969 Cologne, Germany.
Email: mreyers@meteo.uni-koeln.de

Abstract

An unusual dust event over the Atacama Desert occurred in July 2016. Here, a synoptic study of the event is carried out using the NCEP FNL analysis data and WRF-chem simulations. The "zonalization" of a mid-tropospheric trough leads to the formation of a horizontal convergence band over the Northern Atacama and thus downward wind below it. As the descending air masses warm adiabatically, strong temperature contrasts to the colder air over the western Andes occur and intensify the down-valley winds, thus leading to extraordinary strong easterly winds in the Atacama. Simulations with WRF-chem indicate that these surface winds are sufficient for large-scale dust emission, and simulated dust plumes traveling far over the eastern South Pacific agree well with the observations. As the integrated dust load is comparable with the load observed in major dust sources of the world, our findings highlight the importance of such unusual events.

KEYWORDS

analysis, Atacama Desert, dust event, dynamic/processes, simulation, wind

1 | INTRODUCTION

Dust storms are reported and analyzed for many arid and semi-arid regions on Earth, such as North Africa (e.g., Huneeus *et al.,* 2016), Arabian Peninsula (e.g., Notaro *et al.,* 2013), China (e.g., Guo *et al.,* 2018), Central Asia (e.g., Indoitu *et al.,* 2012), and Australia (e.g., Gabric *et al.,* 2010). Severe dust events are usually triggered by large-scale synoptic controls, as high wind speeds over wide areas are required for their development. Qian *et al.* (2001) demonstrate that the dust storm frequency in Northern China is strongly related to surface cyclone activities, while over Australia dust storm occurrence is influenced by the location of the subtropical Indian Ocean high (Ekström *et al.,* 2004). For the Middle East, Hamidi *et al.* (2013) find an interaction between dust storms and the location of surface lows and

highs relative to the dust sources. Furthermore, Saharan dust transport is strongly affected by the North African Dipole Intensity (Cuevas *et al.,* 2017; Rodríguez *et al.,* 2015), while dust activity over southwest Asia is modulated by changes in the mean sea level pressure between the Caspian Sea and Hindu Kush (Kaskaoutis *et al.,* 2016; 2017). Topographic influences on the development of dust storms are detected for an intense dust outbreak in Northern Africa, where lee cyclogenesis east of the Atlas Mountain facilitates the formation of a strong surface cyclone and thus dust mobilization over Algeria (Huneeus *et al.,* 2016).

Over South America, dust storms mainly occur in the western parts of the continent. Prospero *et al.* (2002) identify Patagonia, central-western Argentina, and the Puna-Altiplano Plateau as key dust storm regions. Strong westerly winds during winter are the main driver for dust events in Puna-Altiplano in 2009 and 2010 (Gaiero *et al.,* 2013),

accompanied by anomalous dry conditions associated with El Nino conditions during these years. Dust events originating in Patagonia are related to low pressure perturbations coming from the south, which may generate storms with very high wind speeds (Gasso and Stein, 2007). Hence, as for most other regions of the world, dust storm occurrence over this part of South America is well understood. In contrast, little is known about dust storms over the Atacama Desert. This is probably due to the fact that dust storms in this Desert are very sparse, as they are usually suppressed by the topographic and climatic conditions (see Section 2.1). Despite these limiting factors, a severe dust storm occurred over the Northern part of the Atacama Desert in the morning hours of July 8, 2016, releasing a dense dust plume that traveled far westward over the South Pacific (Figure 1a). Owing to the unusual features of the event, it attracted considerable curiosity in the research community, but to our best knowledge, it is so far not analyzed in detail in a peer-reviewed study. It is, however, useful for several reasons to improve our knowledge on the conditions leading to and the processes involved in such dust events. For instance, climatic archives of the Atacama Desert may be interpreted more reliably once we better understand the dust storm frequency and dust fluxes in this region. Moreover, as dust deposition represents a natural source of nutrients, dust events as the one from 2016 likely affect the biogeochemical cycle in the coastal ocean surface of the Eastern South Pacific.

Regional models are a useful tool to analyze dust storms, as they not only provide information of the dust fluxes on high temporal and three-dimensional spatial resolution but also give insight into local processes involved in the onset and the temporal evolution of the events. Numerous models have been developed in recent years, and evidence is found that they are able to realistically simulate individual dust storms (Hamidi *et al.,* 2014; Yu *et al.,* 2017).

In this study, the severe dust storm that occurred over the Atacama Desert in July 2016 is analyzed. Synoptic analysis data are used to examine the large-scale synoptic conditions initiating this unusual event. In addition, a highly resolved simulation of the dust storm is consulted to specify the small-scale processes which are involved and to demonstrate the singularity of the event.

2 | STUDY AREA, DATA, AND METHODS

2.1 | The study area

The Atacama Desert stretches along the subtropical west coast of South America and is bordered by the South Pacific and the Andes Mountains. It is thus characterized by steep orographic gradients (Figure 1b). A coastal cliff with heights of up to more than 1,000 m asl rises from the ocean in the west, merging into the central Atacama Desert, which is
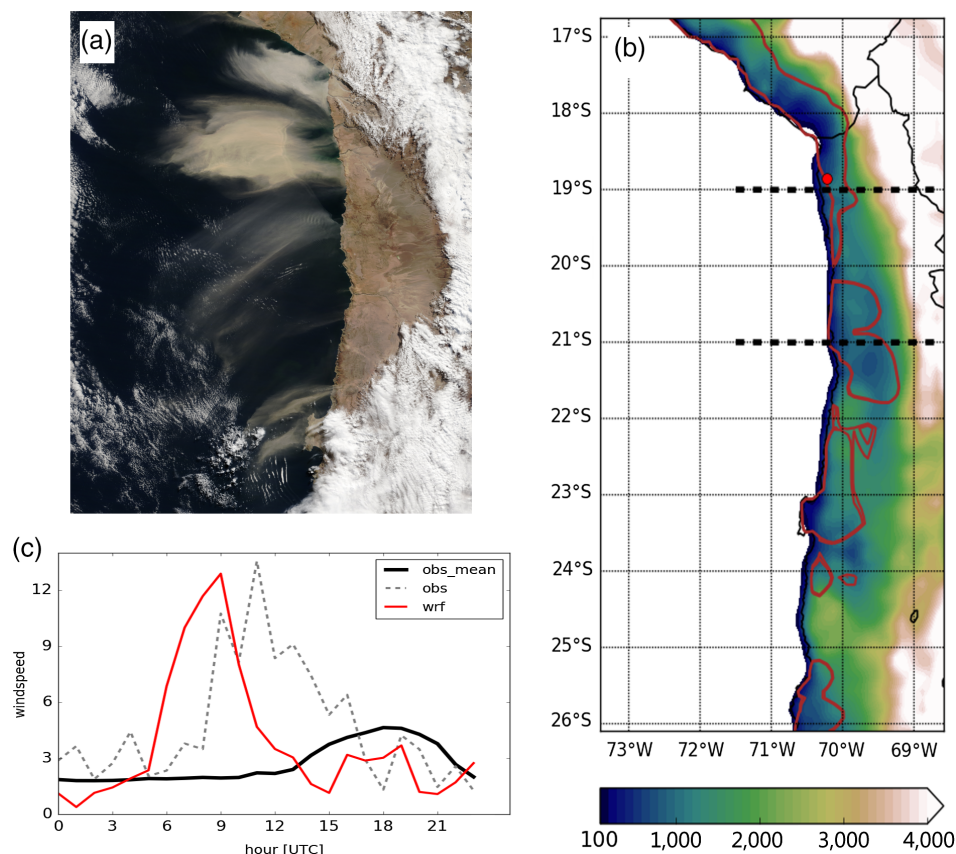

FIGURE 1 (a) MODIS true-color image of the dust plume over the coast of northern Chile on July 8, 2016 (source: https://www.earthobservatory.nasa.gov) (b) model domain and topographic height in m of the WRF simulation. The brownish contours show isolines of the erodability of 0.2, the red dot the location of station CAMA, and the stippled black lines the position of the cross sections represented in the synoptic analysis. (c) Mean observed day course for winter (June–August; black line) and observed time series for July 8, 2016 (gray stippled line) of 10-min averaged 5 m wind speed in ms^{-1} at station CAMA, and WRF simulated time series of 10 m wind speed at the grid point nearest to location of CAMA (red line)

characterized by broad valleys, plains, mountain ranges, and Salars. To the east, the Andes rise to heights of up to 6,000 m asl. The Atacama Desert is one of the driest places on Earth. Its hyper-aridity results from the interplay of a very stable anticyclone over the subtropical eastern South Pacific, the cold Humboldt Current, and the rain shadow effect of the Andes (e.g., Garreaud *et al.,* 2010). In the Central Atacama Desert annual precipitation only amounts to a few millimeters per year on average (Houston, 2006), and it is assumed that in some parts rainfall is absent for decades. Hence, the Atacama Desert can be considered as an area with low humidity and vegetation, and thus an area which may be prone to wind erosion. As synoptic systems are mostly blocked by the Andes and the stable subtropical high, the near-surface wind climate is mainly steered by thermal land-sea contrasts. Nevertheless, wind systems are quite complex due to the topographic features. During the day, when the land surface and in particular the westerly slopes of the Andes are strongly heated, eastward onshore and upslope winds occur. The upslope winds can reach high velocities, but the formation of pronounced dust plumes is suppressed by the steep rise of the Andes. During the night the circulation reverses, thus leading to down-valley nocturnal winds (Munoz *et al.,* 2013; Ruttlant *et al.,* 2013; Jacques-Coper *et al.,* 2015; Munoz *et al.,* 2018). These winds may be strong in stretched valleys and at the higher-elevated slopes of the Andes, but are generally weak in the plains North of 22°S (see Munoz *et al.,* 2018, and our Figure 1c) where the main dust sources are located (Figure 1b). The potential dust sources in the study area are plotted based on the WRF terrestrial database as defined by Ginoux *et al*. (2001) and introduced as erodibility in the model. Hence, despite the extremely dry climate in the Atacama Desert, the development of strong dust events is usually inhibited by the climatic and topographic conditions described above.

2.2 | Data and methods

The NCEP FNL Operational Global Analysis data (National Centers for Environmental Prediction; full reference is given in the reference list) is used in this study for a large-scale synoptic analysis of the 2016 event. This data set is freely available in 6-hourly temporal and 1° by 1° spatial resolution.

High-resolution simulations are performed with the dynamical Weather Research and Forecasting Model (WRF; http://www.wrf-model.org) version 3.9, fully coupled with an online chemistry module (WRF-chem; Grell *et al.,* 2005). Various parameterizations for the physics are available. The model setup used here is described in Appendix S1. The S04 dust scheme (Shao, 2004) is used to calculate the dust emission in the study area. This scheme estimates the threshold

friction velocity of wind erosion, intensity of sand drift, and dust emission rate for predefined particle size groups (see Appendix S1 for details).

Boundary conditions for the WRF-chem simulations are provided by the NCEP FNL Analysis and are updated every 6 hr. A horizontal resolution of 10 km is achieved by a single one way nesting, with 105 grid boxes in South–North direction and 51 grid boxes in the West–East direction, covering the area from 73.5-68.5°W to 26-17°S (see Figure 1a). Furthermore, we use 45 vertical terrain-following eta-levels. The dust storm occurred in the morning hours of July 8, 2016. Hence, we simulate the period from 5 July, 00UTC, to 9 July, 00UTC, using the first day as spin up time.

Wind observations are taken from the solar monitoring station Pampa Camarones (CAMA) installed at 18.8584°S and 70.2173°W in an altitude of 795 m asl (see Figure 1b). The station is part of a database built up in a series of measuring campaigns undertaken by Chile's energy agencies and funded mainly by the Chilean government (Munoz *et al.,* 2018). Amongst other parameters, 10 min averaged wind speed in 5 m is provided for CAMA. The time period with 5 m wind data availability encompasses the years 2012 to 2017. Data for this and more than 40 other stations in the Atacama Desert are publically available at http://walker.dgf.uchile.cl/Mediciones/ (Munoz *et al.,* 2018).

3 | RESULTS

3.1 | Synoptic analysis

The large-scale synoptic conditions in the period before the dust event are characterized by a mid-tropospheric trough over the Eastern South Pacific (Figure 2). When the trough propagates toward South America and approaches the Andes, weak north-northwesterly winds occur at its foreside over Northern Chile. At 06 UTC on 8 July the circulation changes to a rather zonal flow ("zonalization"), leading to a speed up and a slight westerly deflection of the mid-level winds off the coast of Northern Chile (Figure 2d). As at the same time the weak north-northwesterlies at the foreside of the trough persist, this configuration results in a zone of horizontal convergence over the Northern part of the Atacama Desert (Figure 2d).

This mid-tropospheric convergence zone is also visible in the WRF simulations (Figure 3a–c), and has, as will be shown in the following, strong local impacts. The convergence band is moving eastwards and crosses the Northern part of the Atacama Desert within a few hours. Owing to mass conservation, downward low-level vertical winds are generated below the convergence zone (Figure 3d–f). Congruently with the convergence zone, these downdrafts migrate towards the western slopes of the Andes.
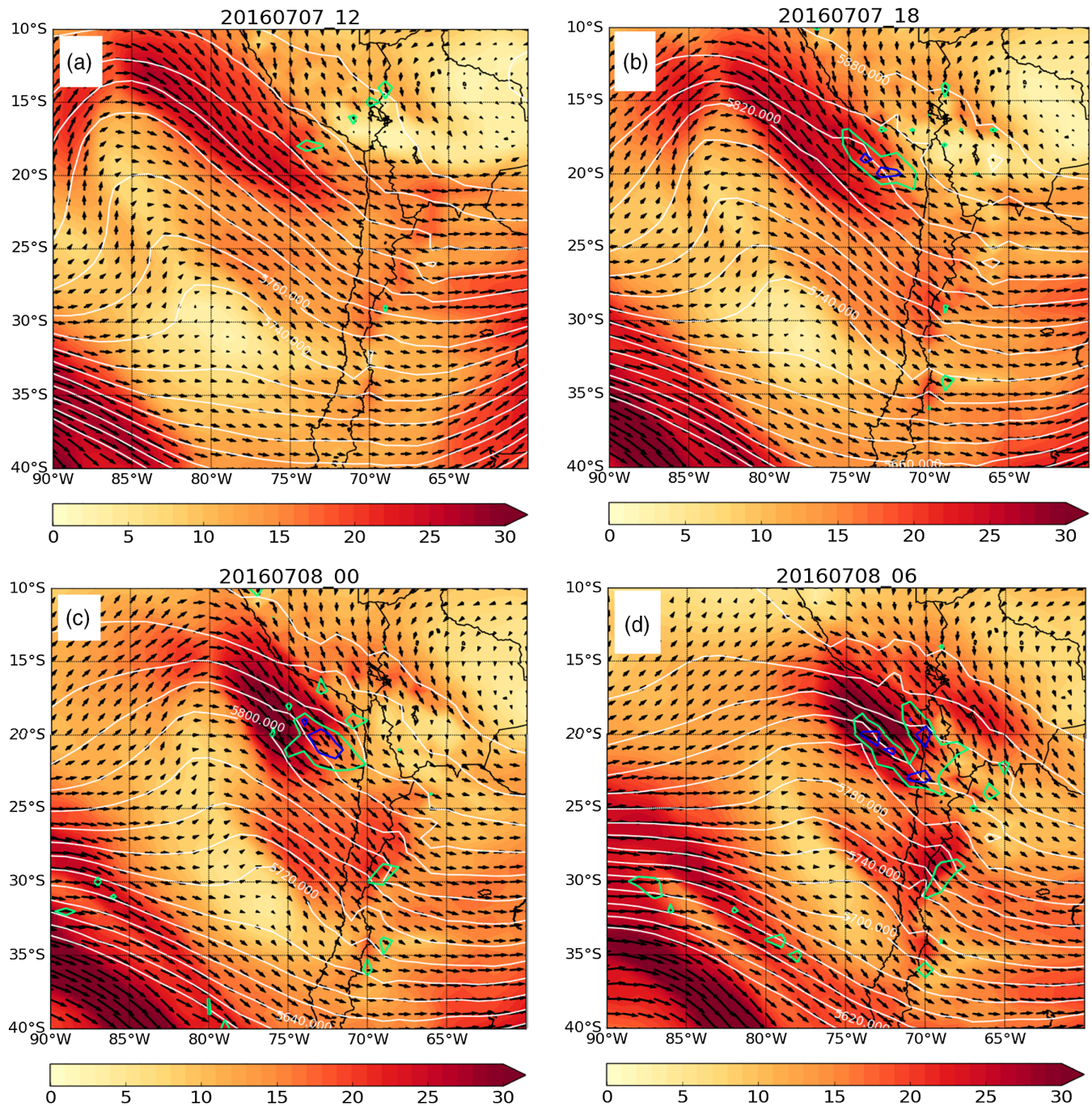
FIGURE 2 Contours of geopotential height (white lines), wind speed in ms^{-1} (shading), and wind direction (black arrows) at 500 hPa in NCEP FNL at (a) 12UTC 07, (b) 18 UTC 07, (c) 00UTC 08, and (d) 06UTC July 8, 2016. The green and blue lines represent isolines of the divergence at 500 hPa of -0.00004 and -0.00008 s^{-1}, respectively

Next, longitude-height cross sections along 19°S (Figure 4; see stippled lines in Figure 1b) and 21°S (Supplementary Figure S1) obtained from the WRF simulation are analyzed. According to the first law of thermodynamics, the descending air masses (white stippled lines in Figure 4a–c) are heated adiabatically. Hence, they are warmer than the surrounding air in equivalent heights (e.g., visible as peaks in the temperature contours at 3000–4000 m asl in Figure 4a,b). As the downdrafts prevail down to the surface,

pools of anomalous high temperature also occur in low levels over the coastal area, while colder air lies over the slope surfaces of the Andes (see peaks in temperature contours at 1500–2500 m asl and troughs east of them in Figure 4b,c). Consequently, air masses over the slope surfaces have a higher density than the air at equivalent levels further west. This results in strong low-level pressure gradients of up to -10 Pa/km between 70.5° and 70°W (i.e., the pressure gradient force is directed from East to West; see Figure 4d–f).
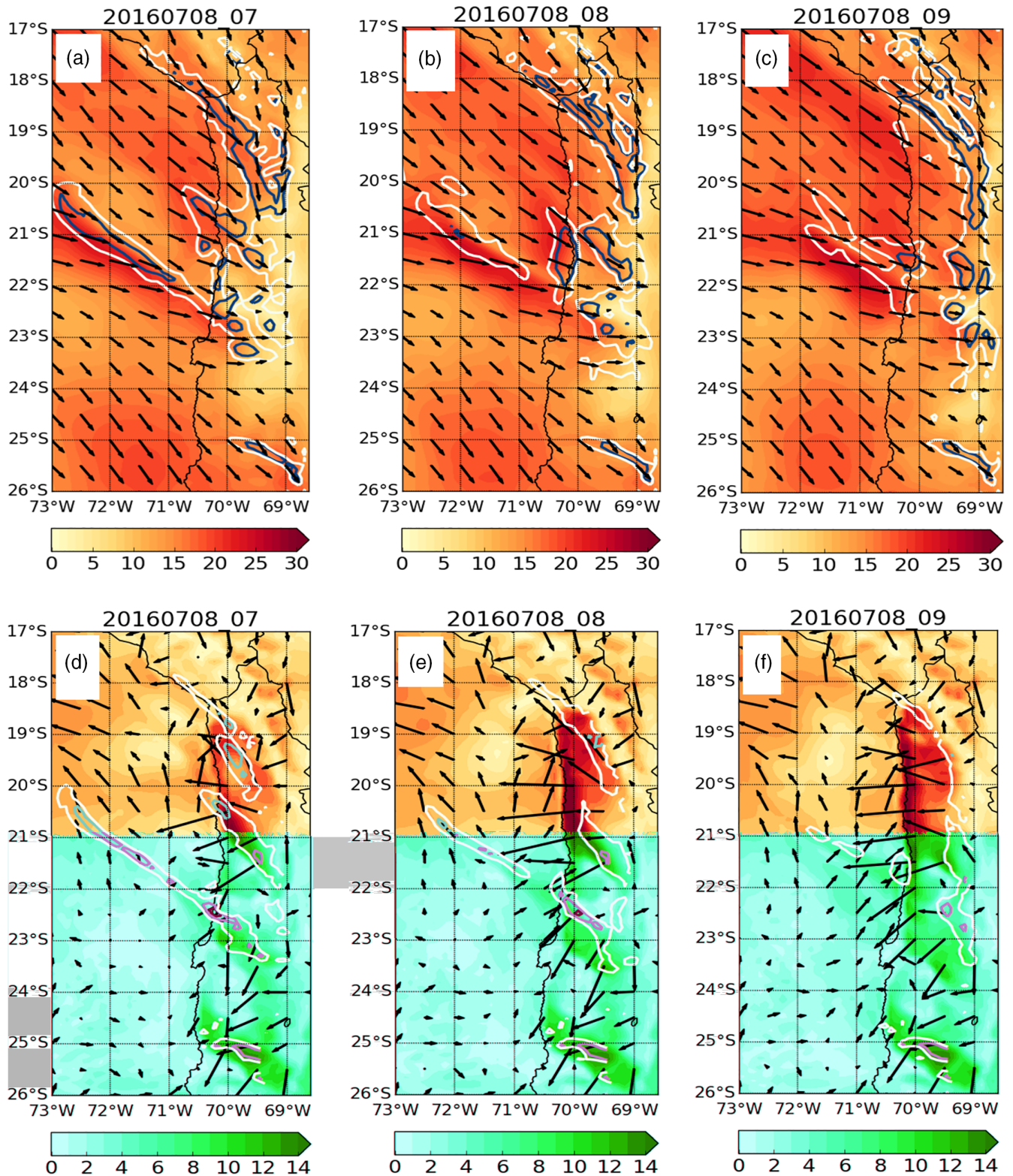
FIGURE 3 (a-c) WRF simulated wind speed in ms^{-1} (shading) and wind direction (black arrows) in 5000 m asl at 07UTC, 08UTC, and 09UTC of July 8, 2016. The white and blue lines represent isolines of the divergence at 5000 m asl of −0.0001 and −0.0002 s^{-1}, respectively. (d-f) WRF simulated 10 m wind speed in ms^{-1} (shading) and wind direction (black arrows) at 07UTC, 08UTC, and 09UTC of July 8, 2016. The white and light blue lines represent isolines of the vertical wind component at 3000 m asl of −0.2 and −0.4 ms^{-1}, respectively. Note that for clarity not all wind arrows are shown
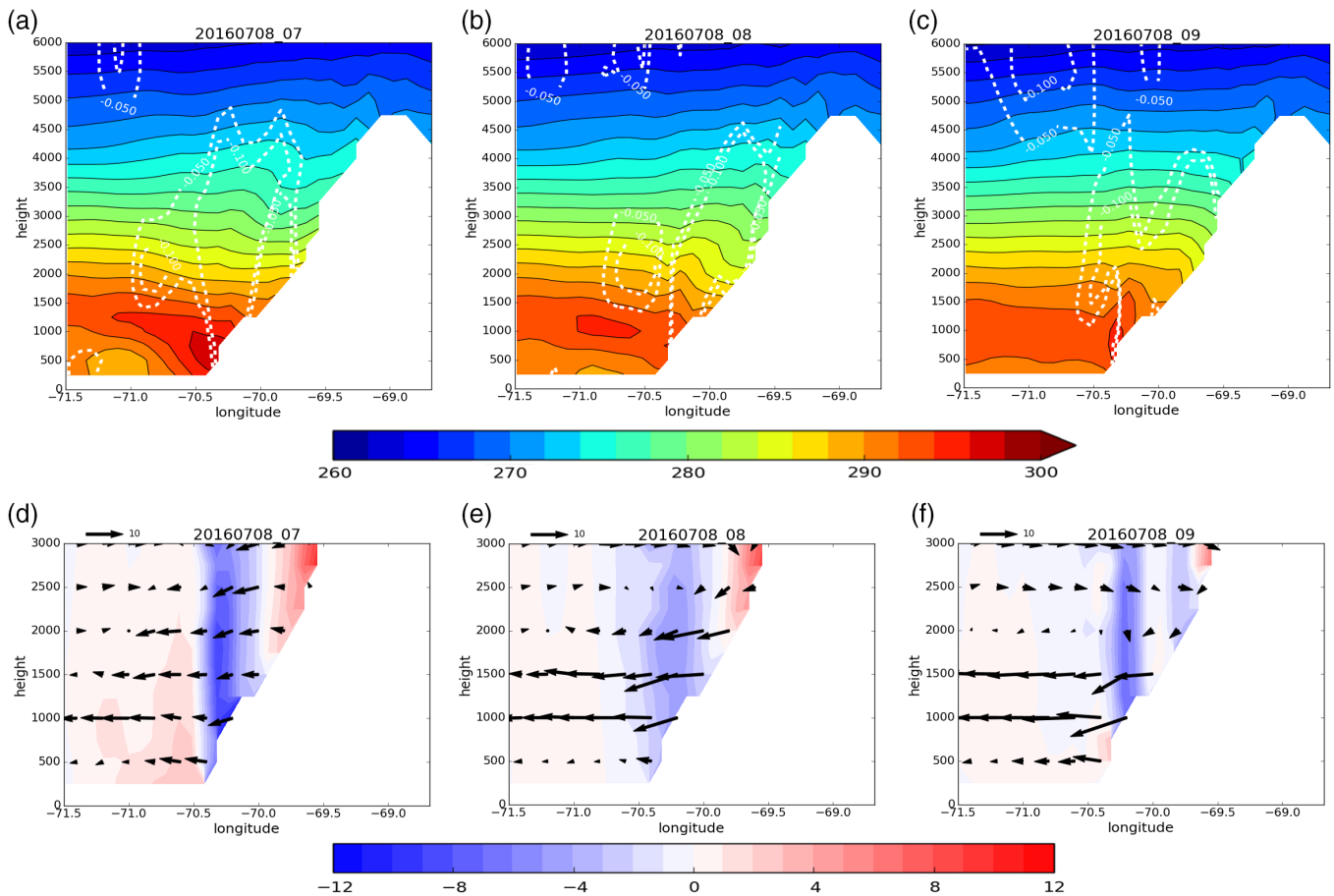
FIGURE 4 (a-c) Longitude-height cross sections of temperature in K (shading) and downward vertical wind component (white stippled contours; shown are contours of -0.05 and -0.1 ms^{-1}) at 07UTC, 08UTC, and 09UTC of July 8, 2016 at 19°S latitude (cf. stippled lines in Figure 1a). (d-f) Longitude-height cross sections of the zonal pressure gradient in pa/km ($-\partial p/\partial x$, shading; negative values represent a pressure gradient forcing which is directed from east to west) and u-w wind components (arrows) at 07UTC, 08UTC, and 09UTC of July 8, 2016. The reference arrow at top left of the panels display a wind speed of 10 ms^{-1}. Note that for clarity arrows are shown every 0.2° longitude and 500 m height and that the w-component is multiplied by factor 10

Hence, the down-valley winds are strongly accelerated when they cross the near-coastal area, and finally westward winds with extraordinary high velocities occur over the plains of the Atacama Desert. Processes are equivalent for the other regions south of 19°S (see Supplementary Figure S1 for 21°S), and strong near-surface winds are thus simulated for a broad coastal band between 19°S and 22°S (up to 15.5 ms^{-1}; see Figure 3e,f). As in the Northern part of the Atacama Desert some regions reveal very low threshold friction velocities of 0.25 ms^{-1} and less (not shown) these wind speeds are sufficient for large-scale dust emission (see section 3.2).

Wind speed observations at CAMA substantiating the extraordinariness of the event are displayed in Figure 1c. The time series for July 8, 2016 reveal a distinct peak at 11UTC, a time of day when winds are usually rather weak at this site (Figure 1c). A maximum 10-min average wind speed of 13.82 ms^{-1} is reported, which is by far the highest velocity measured during 2012–2017. After 11UTC, the observed wind speed rapidly decreases. A similar temporal course is

simulated by the WRF model, although the strong increase and the peak in wind speed is depicted too early (Figure 1c). Another interesting feature is revealed when analyzing temperature observations at CAMA. Due to adiabatic heating (see above) record-high temperatures are observed for July 8, 2016 (see Supplementary Figure S2). A maximum temperature of 34.5°C is found at 18UTC, which is about 15°C warmer than the mean temperature for winter (June–August). These extraordinary high temperatures are simulated realistically by the WRF model, despite an underestimation of the peak temperatures (Supplementary Figure S2). These findings provide evidence that the model is generally suitable to simulate such an extraordinary event.

3.2 | Simulation of the dust event

The WRF-chem model is used for the simulation of the dust event. The quantitative and qualitative verification of the model was performed in an earlier study with observed data
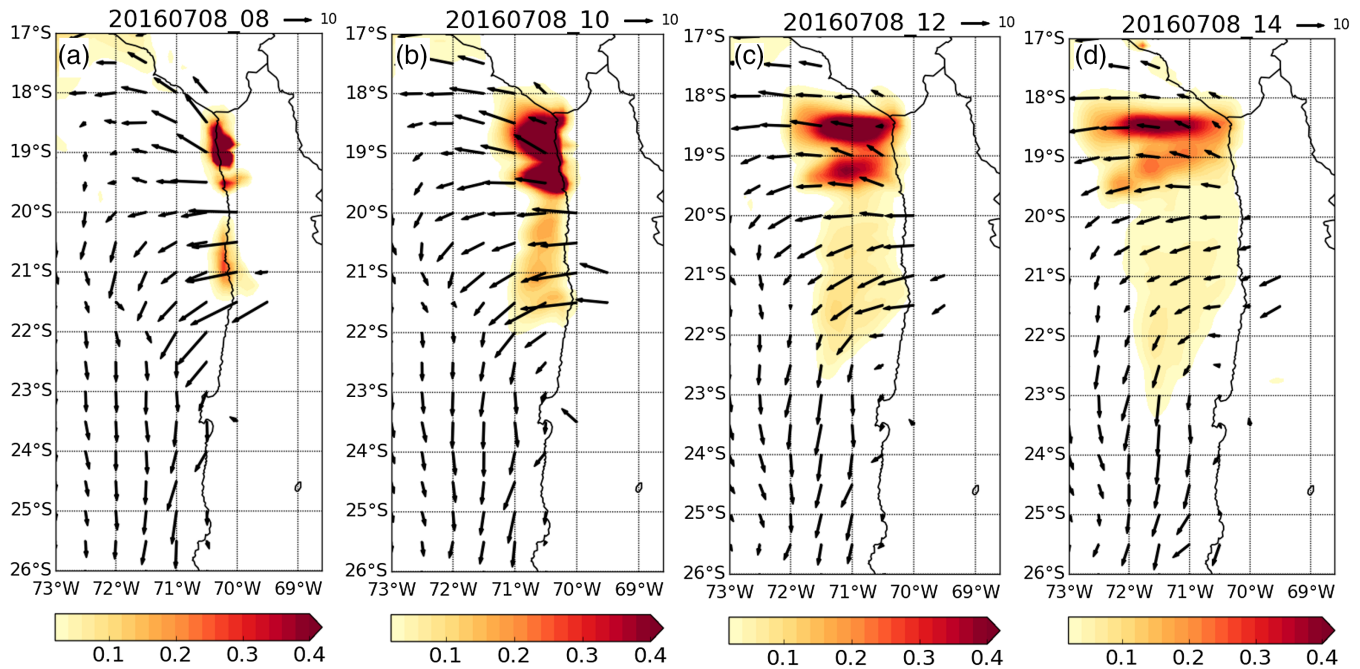
FIGURE 5　Integrated dust load in gm^{-2} (shading) and wind direction in 1000 m asl (arrows) at (a) 08UTC, (b) 10UTC, (c) 12UTC, and (d) 14UTC of July 8, 2016. The reference arrow at top right of the panels display a wind speed of 10 ms^{-1}. Note that for clarity not all wind arrows are shown

(Hamidi *et al.,* 2017). Figure 5 display the simulated dust plume at 08, 10, 12, and 14UTC, respectively. At 08UTC strong dust emission takes place over the Northern part of the Atacama Desert, forming two separated dust plumes (Figure 5a), which is compatible with the simulated strong near-surface winds at this time (Figure 3e). Vertical profiles reveal that the dust remains in altitudes ranging approximately from 500 to 1,000 m asl throughout the subsequent hours (not shown). The dust plumes reach the Pacific Ocean at 10UTC and totally propagate over the ocean until 14UTC. During this period, the dust plume south of 20°S is deflected to the South along with the winds in 1000 m asl, while the dust plume north of 19.5°S is propagated longitudinally (Figure 5b–d). Further, a denser dust plume over 18–19°S rather than 21–22°S is simulated. These results agree well with the plumes in the NASA satellite image for the dust event (Figure 1a), and demonstrate that the dust sources of the area over 18–19°S are more active than the area over 21–22°S.

4 | CONCLUSIONS AND DISCUSSION

In this study, a synoptic analysis of the July 8, 2016 dust event over the Atacama Desert was performed. A "zonalization" of a mid-tropospheric trough over the subtropical Eastern South Pacific was crucial for the development of this event. The results of the WRF-chem simulation show a good consistency with the observations in terms of wind characteristics and the propagation of the dust plumes. The simulated maximum dust emission during the event is comparable to that of some areas which are well-known for high dust activity (e.g., Todd *et al.,* 2008; Shao *et al.,* 2010; Hamidi *et al.,* 2017). Hence, the Atacama Desert has the potential to be a major dust source, not necessarily because of the frequency but because of the intensity of the dust storm.

Owing to its curiosity, the dust event has not gone unnoticed and is hence under discussion in the research community. However, a consensus has not been achieved so far with respect to the synoptic conditions initiating the event. On a public research platform (see https://www.theweathernetwork.com/news/articles/weird-backward-dust-plume-flows-from-driest-place-on-earth/70030) for example it is hypothesized that a convergence zone of an upper level jet streak located over the Atacama Desert facilitated the formation of a high pressure ridge, which pushed strong winds off-shore. This hypothesis could not be confirmed by our findings. Rather, we found that convergence zone associated with the entrance region of the jet streak was located over the Pacific and not over the Atacama Desert (not shown). Hence, it is obvious that a deeper research with respect to this topic is worthwhile. Here, we have focused on atmospheric processes triggering the dust event. A detailed analysis of the model estimates of dust emission, deposition, concentration, and fluxes is subject of ongoing research, and we hope that our study motivates other researchers to focus on this region in

future studies. It would particularly be interesting, why the uncovered mechanisms operate with such intensity only in this event, and whether this event is rather unique or whether dust storms occur frequently, not only under present climate conditions but also in the paleo- or future climate. For example, Lambert *et al.* (2015) found that dust fluxes over the Eastern South Pacific were much higher during the LGM than in the Holocene, which is exactly the region where the majority of dust is transported by the dust storm studied here. To obtain dust emission and flux climatologies, long-term dust simulations are required. With this respect it should be taken into account in future studies that the simulation of the complex processes involved in the dust event studied here may be quite sensitive to the boundary conditions and the model setup. While the results are similar when using ERA-Interim instead of NCEP FNL as boundary conditions (not shown), they strongly depend on the size of the model domain. When we enlarge the domain, the simulated dust emission strongly decreases. This is due to the fact that discrepancies between the Analysis data and the WRF simulated atmospheric fields may be enhanced within the enlarged model domain, as information from the Analysis data are nudged into the model domain only at the boundaries. As a consequence the mid-tropospheric convergence zone is not captured accurately by the regional model and near-surface winds are much weaker than in the simulations with the original model domain (Supplementary Figure S3). These findings indicate at the same time that this convergence band is indeed the pivotal process for the development of the dust event.

ACKNOWLEDGEMENTS

ORCID

Mark Reyers https://orcid.org/0000-0001-7085-9345

REFERENCES

Cuevas, E., Gomez-Pelaez, A.J., Rodríguez, S., Terradellas, E., Basart, S., García, R.D., García, O.E. and Alonso-Perez, S. (2017) The pulsating nature of large-scale Saharan dust transport as a result of interplays between mid-latitude Rossby waves and the north African dipole intensity. *Atmospheric Environment*, 167, 586–602. https://doi.org/10.1016/j.atmosenv.2017.08.059.

Ekström, M., McTainsh, G.H. and Chappell, A. (2004) Australian dust storms: temporal trends and relationship with synoptic pressure distributions (1960-1999). *International Journal of Climatology*, 24 (12), 1581–1599. https://doi.org/10.1002/joc.1072.

Gabric, A.J., Cropp, R.A., McTainsh, G.H., Johnston, B.M., Butler, H., Tilbrok, B. and Keywood, M. (2010) Australian dust storms in 2002-2003 and their impact on Southern Ocean biogeochemistry. *Global Biogeochemical Cycles*, 24, GB2005. https://doi.org/10.1029/2009GB003541.

Gaiero, D.M., Simonella, L., Gasso, S., Gili, S., Stein, A.F., Sosa, P., Becchio, R., Arce, J. and Marelli, H. (2013) Ground/satellite observations and atmospheric modelling of dust storms originating in the high Puna-Altiplano deserts (South America): implications for the interpretation of paleo-climatic archives. *Journal of Geophysical Research: Atmosphere*, 118, 3817–3831. https://doi.org/10.1002/jgrd.50036.

Garreaud, R.D., Molina, A. and Farias, M. (2010) Andean uplift, ocean cooling and Atacama hyperaridity: a climate modelling perspective. *Earth and Planetary Science Letters*, 292(1), 39–50. https://doi.org/10.1016/j.epsl.2010.01.017.

Gasso, S. and Stein, A.F. (2007) Does dust from Patagonia reach the sub-Antarctic Atlantic Ocean? *Geophysical Research Letters*, 34 (1), L01801. https://doi.org/10.1029/2006GL027693.

Ginoux, P., Chin, M., Tegen, I., Prospero, J.M., Holben, B., Dubovik, O. and Lin, S.J. (2001) Sources and distributions of dust aerosols simulated with the GOCART model. *Journal of Geophysical Research*, 106(D17), 20255–20273.

Grell, G.A., Peckham, S.E., Schmitz, R., McKeen, S.A., Frost, G., Skamarock, W. and Eder, B. (2005) Fully-coupled online chemistry within the WRF model. *Atmospheric Environment*, 39, 6957–6975. https://doi.org/10.1016/j.atmosenv.2005.04.027.

Guo, L., Fan, B., Zhang, F., Jin, Z. and Lin, H. (2018) The clustering of severe dust storm Occurence in China from 1958 to 2007. *Journal of Geophysical Research: Atmosphere*, 123(15), 8035–8046. https://doi.org/10.1029/2018JD029042.

Hamidi, M., Kavianpour, M.R. and Shao, Y. (2013) Synoptic analysis of dust storms in the Middle East. *Asia-Pacific Journal of Atmospheric Sciences*, 49(3), 279–286. https://doi.org/10.1007/s13143-013-0027-9.

Hamidi, M., Kavianpour, M.R. and Shao, Y. (2014) Numerical simulation of dust events in the Middle East. *Aeolian Research*, 13, 59–70. https://doi.org/10.1016/j.aeolia.2014.02.002.

Hamidi, M., Kavianpour, M.R. and Shao, Y. (2017) A quantitative evaluation of the 3–July 8, 2009 Shamal dust storm. *Aeolian Research*, 24, 133–143.

Houston, J. (2006) Variability of precipitation in the Atacama Desert: its causes and hydrological impact. *International Journal of Climatology*, 26, 2181–2198. https://doi.org/10.1002/joc.1359.

Huneeus, N., Basart, S., Fiedler, S., Morcrette, J.-J., Benedetti, A., Mulcahy, J., Terradellas, E., Pérez García-Pando, C., Pejanovic, G., Nickovic, S., Arsenovic, P., Schulz, M., Cuevas, E., Baldasano, J. M., Pey, J., Remy, S. and Cvetkovic, B. (2016) Forecasting the northern African dust outbreak towards Europe in April 2011: a model intercomparison. *Atmospheric Chemistry and Physics*, 16, 4967–4986. https://doi.org/10.5194/acp-16-4967-2016.

Indoitu, R., Orlovsky, L. and Orlovsky, N. (2012) Dust storms in Central Asia: spatial and temporal variations. *Journal of Arid Environments*, 85, 62–70. https://doi.org/10.1016/j.jaridenv.2012.03.018.

Jacques-Coper, M., Falvey, M. and Munoz, R.C. (2015) Inter-daily variability of a strong thermally-driven wind system over the Atacama Desert of South America: synoptic forcing and short-term predictability using the GFS global model. *Theoretical and Applied Climatology*, 121, 211–223. https://doi.org/10.1007/s00704-014-1231-y.

Kaskaoutis, D.G., Houssos, E.E., Rashki, A., Francois, P., Legrand, M., Goto, D., Bartzokas, A., Kambezidis, H.D. and Takemura, T. (2016) The Caspian Sea–Hindu Kush index (CasHKI): a regulatory factor for dust activity over Southwest Asia. *Global and Planetary Change*, 137, 10–23. https://doi.org/10.1016/j.gloplacha.2015.12.011.

Kaskaoutis, D.G., Rashki, A., Houssos, E.E., Legrand, M., Francois, P., Bartzokas, A., Kambezidis, H.D., Dumka, U.C., Goto, D. and Takemura, T. (2017) Assessment of changes in atmospheric dynamics and dust activity over Southwest Asia using the Caspian Sea–Hindu Kush index. *International Journal of Climatology*, 37, 1013–1034. https://doi.org/10.1002/joc.5053.

Lambert, F., Tagliabue, A., Shaffer, G., Lamy, F., Winckler, G., Farias, L., Gallardo, L. and De Pol-Holz, R. (2015) Dust fluxes and iron fertilization in Holocene and last glacial maximum climates. *Geophysical Research Letters*, 42, 6014–6023. https://doi.org/10.1002/2015GL064250.

Munoz, R.C., Falvey, M., Arancibia, M., Astudillo, V., Elgueta, J., Ibarra, M., Santana, C. and Vasquez, C. (2018) Wind energy exploration over the Atacama Desert: a numerical model-guided observational program. *Bulletin of the American Meteorological Society*, 99, 2079–2092. https://doi.org/10.1175/BAMS-D-17-0019.1.

Munoz, R.C., Falvey, M.J., Araya, M. and Jacques-Coper, M. (2013) Strong Down-Valley low level jets over the Atacama Desert: observational characterization. *Journal of Applied Meteorology and Climatology*, 52, 2735–2752. https://doi.org/10.1175/JAMC-D-13-063.1.

National Centers for Environmental Prediction/National Weather Service/NOAA/U.S. Department of Commerce. (2000). *NCEP FNL Operational Model Global Tropospheric Analyses, continuing from* July 1999. Research data archive at the National Center for Atmospheric Research, Computational and Information Systems Laboratory. Available at: https://doi.org/10.5065/D6M043C6 [Accessed 8th August 2018].

Notaro, M., Alkolibi, F., Fada, E. and Bakhrjy, F. (2013) Trajectory analysis of Saudi Arabian dust storms. *Journal of Geophyiscal Research: Atmosphere*, 118, 6028–6043. https://doi.org/10.1002/jgrd.50346.

Prospero, J.M., Ginoux, P., Torres, O., Nicholson, S.E. and Gill, E. (2002) Environmental characterization of global sources of atmosphere soil dust identified with the Nimbus 7 total ozone mapping spectrometer (TOMS) absorbing aerosol product. *Review of Geophysics*, 40(1), 2–1. https://doi.org/10.1029/2000RG00095.

Qian, W., Quan, L. and Shi, S. (2001) Variations of the dust storm in China and its climatic controls. *Journal of Climate*, 15, 1216–1229. https://doi.org/10.1775/1520-0442(2002)015.

Rodríguez, S., Cuevas, E., Prospero, J.M., Alastuey, A., Querol, X., López-Solano, J., García, M.I. and Alonso-Pérez, S. (2015) Modulation of Saharan dust export by the north African dipole. *Atmospheric Chemistry and Physics*, 15, 7471–7486. https://doi.org/10.5194/acp-15-7471-2015.

Ruttlant, J.A., Munoz, R.C. and Garreaud, R.D. (2013) Meteorological observations on the northern Chilean coast during VOCALS-rex. *Atmospheric Chemistry and Physics*, 13, 3409–3422. https://doi.org/10.5194/acp-13-3409-2013.

Shao, Y. (2004) Simplification of a dust emission scheme and comparison with data. *Journal of Geophysical Research*, 109, D10202. https://doi.org/10.1029/2003JD004372.

Shao, Y., Fink, A.H. and Klose, M. (2010) Numerical simulation of a continental scale Saharan dust event. *Journal of Geophysical Research*, 115, D13205. https://doi.org/10.1029/2009JD012678.

Todd, M.C., Bou Karam, D.C., Cavazos, B.C., Heinold, B., Baldasano, J.M., Cautenet, G., Koren, I., Perez, C., Solmon, F., Tegen, I., Tulet, P., Washington, R. and Zakey, A. (2008) Quantifying uncertainty in estimates of mineral dust flux: an intercomparison of model performance over the Bodélé depression, northern Chad. *Journal of Geophysical Research*, 113, D24107. https://doi.org/10.1029/2008JD010476.

Yu, X., Wang, T., Liu, C. and Pu, L. (2017) Numerical studies on a severe dust storm in East Asia using WRF-Chem. *Atmospheric and Climate Sciences*, 7(1), 92–116. https://doi.org/10.4236/acs.2017.71008.

SUPPORTING INFORMATION

Additional supporting information may be found online in the Supporting Information section at the end of this article.